ACS APPLIED NANO MATERIALS

Article

Cite This: ACS Appl. Nano Mater. 2019, 2, 4954−4967

www.acsanm.org

Bioinspired Alkoxysilane Conservation Treatments for Building Materials Based on Amorphous Calcium Carbonate and Oxalate Nanoparticles

A. Burgos-Cara, C. Rodríguez-Navarro, M. Ortega-Huertas, and E. Ruiz-Agudo*

Department of Mineralogy and Petrology, University of Granada, 18071 Granada, Spain

Supporting Information

ABSTRACT: The weathering of building and sculptural stone due to increasing air pollution and salt damage results in the loss of invaluable cultural heritage artworks. This has prompted the design and application of novel and effective conservation treatments. Here, we study the effect of amorphous calcium carbonate (ACC) and oxalate (ACO) nanoparticles synthesized through an emulsion-assisted precipitation on alkoxysilane-based products, commonly used for the conservation of cultural heritage. Mimicking the mechanisms by which biominerals form via amorphous precursors and natural surfaces achieve high hydrophobicity through surface roughness (e.g., lotus leaf), alkoxysilane gels dosed with ACC and ACO nanoparticles were applied on different non-silicate substrates (marble, calcarenite, and gypsum). Our results show that this bioinspired approach for enhancing the performance of alkoxysilane-based treatments could be suitable for the protection of the aforementioned type of materials, as it has a limited aesthetic impact and negligible effects on hydric and water-vapor transport properties, while it foster compatibility with non-silicate surfaces, preventing drying crack development, enhancing resistance to acid attack, and increasing hydrophobicity due to nanoparticle-induced surface roughness. Best results were obtained using ACO nanoparticles.

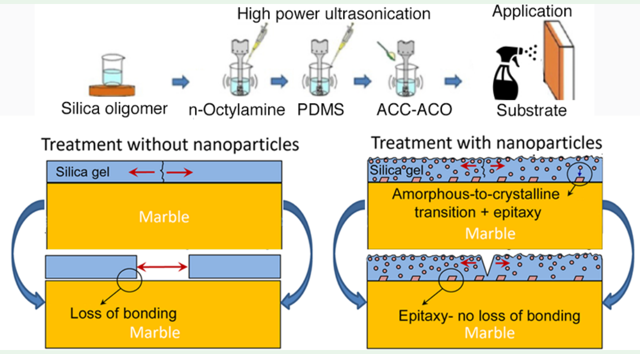

KEYWORDS: *bioinspired treatment, nanoparticles, surface protection, hydrophobicity, alkoxysilane*

1. INTRODUCTION

The built and sculptural heritage is affected by a range of weathering processes that endanger its survival. These include but are not limited to (i) freeze/thaw cycles that generate stress inside porous materials, (ii) mineral dissolution which is accelerated by the presence of air pollution-derived acids, and (iii) mobilization of salts resulting in their punctual accumulation and subsequent in-pore precipitation inducing stresses inside the material. Numerous conservation treatments, including hydrophobic protective coatings and/or consolidants that fill cracks or cement loose grains, have been proposed and implemented over the past decades aiming at strengthening the building material and halting or reducing the impact of such deleterious processes, which typically involve the presence of water or aqueous solutions.[1]

Most protective/consolidant treatments are based on the application of either inorganic (e.g., nanolimes, oxalates, and phosphates among others[2−5]) or organic and silico-organic products (e.g., epoxy, silicon and acrylic resins, and alkoxysilanes, among others[1,6]) to damaged stone, bricks, and/or mortar and plaster surfaces. In particular, alkoxysilanes have found extensive application in the consolidation of stone monuments and other artworks, also presenting protective hydrophobicing properties.[7−9] There are, however, several shortcomings associated with the application of alkoxysilanes in heritage conservation.[10] One is the fact that alkoxysilanes do not form primary bonds between the Si−OH groups and non-silicate surfaces.[1] The second drawback of alkoxysilanes is associated with the pervasive cracking that takes place during the drying of the silica gel. Drying cracks strongly diminish the mechanical (strengthening) properties of alkoxysilane consolidants. Finally, although alkylalkoxysilanes have shown promising effects as protective coatings, their hydrophobicity is limited.[9] Several approaches have been proposed to overcome these important limitations. These include the use of additives (e.g., polydimethylsiloxane, *n*-octylamine, and nanoparticles)[11−14] that could play a dual role as anticracking agents[15] and as hydrophobic functionalities or even as hydrophobic enhancers[8,12,16] (not necessarily related to chemical effects but to increased surface roughness; see below). In the absence of PDMS and *n*-octylamine drying cracks systematically form following sol−gel transition and the resulting cracked surface layer loses any protective or consolidating effect.[11−15] If such additive(s) could also act as

Received: May 14, 2019
Accepted: July 18, 2019
Published: July 18, 2019

DOI: 10.1021/acsanm.9b00905
ACS Appl. Nano Mater. 2019, 2, 4954−4967

coupling agent between the silicate gel and non-silicate substrates (e.g., limestone or marble), some of the above-mentioned drawbacks would be overcome. This, however, remains a big challenge.

Nature can be a source of inspiration for the search of solutions to the problems faced by conservators. Over the past decades, research on biological surfaces has shown that they display multiple unusual properties and functionality, such as water repellency, high and adjustable adhesion, and non-reflective properties, among others.[17] The structure−function characteristics of such natural surfaces can be an inspiration in the development of novel, more efficient materials and treatments for the conservation of cultural heritage. Biological surfaces have been the focus of research aimed at elucidating how nature solves a range of engineering problems and to use these solutions in the design of novel materials and surfaces with selected properties.[17] In this context, attempts to mimic natural structure−property relationships and designs for the generation of weathering-resistant, water-repellent surfaces, not only for conservation purposes but also with industrial applications, have been reported.[18]

The systematic study of the hierarchical microstructure of water-repellent biostructures has shown that microroughness leads to the nonwetting and self-cleaning properties of many living organisms.[17] It has been observed that microroughness changes the contact angle from a Young−Laplace to a Wenzel and Cassie−Baxter regime,[19−21] leading to superhydrophobicity, as occurs in the case of the lotus leaves[22] or the mosquito eyes.[23] On the basis of this gained knowledge, it has been hypothesized that increasing the surface roughness of building materials at the nano- and microscale will ultimately lead to a hierarchical two-scale surface roughness that would result in enhanced hydrophobic behavior.[16,19,23] This can be achieved by applying nanoparticles to the surface of the material to be protected. Nanoparticles have been already used for conservation purposes, including TiO_2 nanoparticles, which display self-cleaning properties,[8,24,25] nanosilica (SiO_2),[26−28] nanoalumina (Al_2O_3),[29] or even tin oxide (SnO_2) nanoparticles,[30] as well as calcium oxalate monohydrate (whewellite)[31] and mixtures of amorphous and crystalline calcium oxalate nanoparticles.[16] These nanoparticles have been applied in combination with a wide range of alkoxysilane-derived formulations or products, and all of them have been shown to be effective anticracking additives[30,32] and, in some cases, hydrophobic enhancers.[16,19,29,30] Despite the foreseen potential of these treatments and the reported effects of nanoparticle addition to alkoxysilanes, their applicability and effectiveness for the protection of building materials need to be fully elucidated. Moreover, additional, improved functional characteristics of the nanoparticle-based treatments, such as better bonding to non-silicate substrates and resistance against chemical weathering (e.g., acid attack), are desirable aspects that have not been explored yet.

Amorphous calcium carbonate and oxalate (ACC and ACO, respectively) nanoparticles are known to play a key role on several biomineralization processes[33−35] as well as many other crystallization processes,[36] as they are key metastable precursor phases preceding the development of crystalline mineral phases which form following nonclassical nucleation pathways.[35−39] In this context, they are tested here as a feasible and effective bioinspired approach to overcome some of the aforementioned limitations of alkoxysilane-based conservation treatments (i.e., development of drying cracks and poor bonding to non-silicate substrates) and to confer additional functionalities, such as enhanced hydrophobicity linked to their microroughness effects. Amorphous inorganic phases are receiving an increasing research interest, as they are present in almost all biomineralization processes.[34] For conservation purposes, the higher solubility of amorphous phases compared to their crystalline counterparts may help to introduce larger amounts of precursors inside stone materials compared to other frequently used treatments such as limewater.[40,41] It will also include a reactive (soluble material) that would eventually dissolve and reprecipitate forming a stable crystalline phase. The molar volume, V_M, of amorphous phases is larger than that of their corresponding crystalline phases (e.g., $V_{M\ calcite} \approx 36$ $cm^3\ mol^{-1}$ vs $V_{M\ ACC} \approx 73$ $cm^3\ mol^{-1}$ [42]). This is advantageous from a conservation point of view because during the amorphous-to-crystalline conversion porosity would be generated in the treatment layer, thereby resulting in enhanced water vapor permeability. The latter is a key parameter to take into account in all conservation interventions because the formation of impervious treatment layers systematically leads to enhanced substrate damage.[1] On the other hand, if the amorphous phases used in these treatments convert into crystalline phases with a crystal structure similar or very similar to that of the minerals constituting the materials to be treated, a strong cohesion (epitaxy) between the treatment and the substrate is expected. This is the case of ACC and calcitic or gypsum substrates,[43] as well as ACO and calcitic substrates. In this way, ACC and ACO (upon their crystallization into stable, crystalline phases) might act as coupling agents between silica gels and non-silicate substrates after its recrystallization into mineral phases with an epitaxial relationship to the calcitic substrate.[2,44,45]

The main goal of our study was to investigate the properties that both calcium carbonate and calcium oxalate, applied as amorphous nanoparticles, confer to Si-coatings based on standard tetraethoxysilane (TEOS) and prepolymerized TEOS (Dynasilan 40) currently used in cultural heritage conservation. We evaluated the effectiveness of these treatments following their application on common non-silicate building materials such as marble, porous calcarenite, and gypsum plaster. In particular, we studied the treatment-induced changes on surface texture, hydrophobic behavior, resistance against acid attack, material color changes, hydric properties, and mechanical properties of treated supports in order to quantify the efficacy and durability of the bioinspired nanoparticle-based treatments.

2. MATERIALS AND METHODS

2.1. Synthesis and Characterization of Amorphous Nanoparticles. Several methods for the synthesis of amorphous nanoparticles have been reported.[46−48] Among these, those based on emulsion-assisted precipitation[46,49,50] lead to amorphous nanoparticles covered by the emulsifying agent. In this work, nanoparticles were produced by mixing 100 mM $CaCl_2$ solution and 100 mM $H_2C_2O_4$ or Na_2CO_3 solution in a 1/1 vol ratio in order to obtain a precipitate of amorphous calcium oxalate (ACO) or amorphous calcium carbonate (ACC), respectively. Polydimethylsiloxane (PDMS) was added to all the aforementioned solutions at a 1/100 (v/v) ratio. As PDMS is immiscible with water, vigorous stirring and sonication were applied to solutions in order to obtain a homogeneous PDMS/solution emulsion and to promote the subsequent emulsion-assisted nanoparticle precipitation.[50] Afterward, the above-mentioned emulsions were quickly mixed and, in less than 3 s, the reaction between both $CaCl_2$ and Na_2CO_3 or $H_2C_2O_4$

emulsions was stopped by adding isopropanol in a 10/1 (v/v) ratio under vigorous stirring. Isopropanol induced a reduction in water activity that favored the stabilization of amorphous phases.[51,52] Stabilization (i.e., inhibition of amorphous-to-crystalline transformation) was also favored by the presence of PDMS, which tended to cover the precipitated nanoparticles (see below), thereby inducing steric hindrance that prevented aggregation. Afterward, suspensions were centrifuged at 1200 rpm for 10 min, and solids were separated from supernatant solution, washed with isopropanol, and centrifuged again before storage. All reagents were purchased from Sigma-Aldrich with a purity of ≥99% according to ACS Reagent grade, and solutions were made using ultrapure water (type I+, resistivity 18.2 MΩ cm, Milli-Q). Formation of amorphous phases was confirmed by powder X-ray diffraction (XRD) using a X'Pert PRO diffractometer (Panalytical, Eindhoven, The Netherlands). The following working conditions were used: radiation Cu Kα ($\lambda = 1.5405$ Å), voltage 45 kV, current 40 mA, scanning angle (2θ) 3−60°, and goniometer speed 0.1° 2θ s^{-1}. Nanoparticles were examined by transmission electron microscopy (TEM) using a Titan (FEI, Oregon, USA) and a CM-20 (FEI-Philips, Amsterdam, The Netherlands) in the case of ACC and ACO nanoparticles, respectively. Nanoparticles were resuspended in ethanol and collected from the reaction media using directly the TEM grid. To analyze the distribution of PDMS on and/or within ACC nanoparticles, maps of Si and Ca present in PDMS and ACC/ACO, respectively, were obtained on the Titan TEM using high-angle annular dark-field (HAADF) images collected in STEM mode and energy dispersive X-ray spectroscopy (EDS) analyses.

2.2. Synthesis of Sols. Sols were prepared using either a commercial monomeric tetraethyl orthosilicate (TEOS) with reagent grade quality (>98%) which had a silicon content of ∼28 wt %, calculated as mass percent of SiO_2 upon complete hydrolysis, or a partially prepolymerized TEOS (Dynasilan 40, Evonik) with a repeating unit between 5 and 7 $-SiO(OR)_2-$ groups and a higher silicon content of about 40 wt % also expressed as SiO_2 present following complete hydrolysis. Hydroxyl-terminated PDMS with a viscosity of ∼ 25 cSt, and an average molecular weight of 550 g mol^{-1} was used as hydrophobic agent and as a promoter for the sol−gel transition due to its role in reducing gelation times.[14] *n*-Octylamine (>99% purity) was employed as an anticracking agent and as a basic catalyst.[28,53] All reactants were purchased from Sigma-Aldrich except Dynasylan 40 that was kindly provided by Evonik. The different treatment groups were noted as TPO and DPO in reference to their composition and were prepared using very similar molar ratios as those previously reported:[12,54] TPO-group treatment included TEOS/PDMS/H_2O/ethanol/*n*-octylamine in molar ratios 1/0.04/4/4/0.00052 and DPO-group treatment included Dynasylan 40/PDMS/*n*-octylamine in molar ratios 1/0.04/0.00052. While the first treatment (TPO) is based on standard TEOS formulation with a lower silica content that imparts a lower viscosity (thereby enhancing penetration), it has the drawback of producing a less dense amorphous silicate protective layer. In contrast, the second alkoxysilane is a commercial and widely available conservation treatment (Dynasilan 40) for stone protection. By inclusion of a higher silica content, the product is more viscous and usually presents a lower penetration. The positive part of this commercial formulation is that, in theory, it would produce a denser and stronger silica gel. By selecting these two products as the TEOS base for our treatments, we wanted to evaluate the role of silica content and associated sol viscosity and density on the performance of our modified TEOS-based protective coating. Note that the silica content and prepolymerization degree of TEOS are critical parameters controlling viscosity, penetration, sol−gel transition, and final product density.[9] Reactants were added to a beaker placed in an ultrasonic bath (Ultrasons 150W, JP SELECTA, Barcelona, Spain) in the same order as written. Gels were stirred and sonicated for 10 min after the last reactant was added in order to promote the homogenization of the mixture. Amorphous nanoparticles, prepared as described above, were added to beakers of the different synthesized sols placed in the ultrasonic bath (i.e., TPO and DPO) in a 5% w/v and noted as −Ca or −Ox in the case of ACC and ACO, respectively (i.e., for TPO group, TPOCa and TPOOx; for DPO group, DPOCa and DPOOx). Such a nanoparticle concentration was selected based on previous results by Manoudis and co-workers,[30] who found that SiO_2 and TiO_2 nanoparticles added to TEOS in such a concentration led to an optimal enhancement of static contact angles (i.e., hydrophobic behavior).

2.3. Preparation of Selected Building Materials. Some of the most common building materials used worldwide since ancient times for construction and ornamental purposes were selected to evaluate the performance of the aforementioned protection/consolidation treatments: white marble, calcarenite (biomicritic limestone), and gypsum plaster. Each of them presents differences in their porous network. White marble from Macael (Almería, Spain), frequently found in monuments of Southern Spain,[55] has the lowest porosity (∼1.8%)[2,56] of the selected materials. Santa Pudia calcarenite has been widely used to build the most significant historic buildings in the city of Granada (Spain).[57] Nonetheless, its bioclastic nature, high porosity (∼30%), coarse pore size, and low degree of cementation limit its durability.[58] Finally, gypsum has been used in several historic buildings, as exemplified by the plasterworks in the Alhambra[59] (Granada, Spain). Gypsum plaster shows the highest porosity (up to 50%) of all materials tested in the present study, and it is the most prone to deterioration.

Test cubes (side = 2 cm) and test slabs (4.5 cm × 4.5 cm × 1 cm) were prepared for all three substrates. Marble samples were prepared from raw quarry blocks from Macael (Almería, Spain). Calcarenite samples were quarried at La Escribana (Granada, Spain). Gypsum samples were prepared from a commercial plaster of Paris by mixing thoroughly 1 kg of gypsum powder with 750 mL of water for 5 min. Then, the paste was cast on a 20 cm × 30 cm × 5 cm plastic container and allowed to set and harden for 3 days before preparation of the gypsum test samples with the above-mentioned dimensions.

2.4. Application of the Gels Containing Amorphous Nanoparticles. Freshly prepared sols were sprayed (∼250 μL/cm^2) over all sample surfaces (except the bottom ones) and left to dry and harden at room conditions (21 ± 2 °C, ∼50% RH) for 1 month prior to further testing. Immersion and pouring application methods were also tested in preliminary experiments, and similar results as in the case of spray application were found in the final products regarding their hydrophobic behavior. However, thicker and less homogeneous coatings were observed following immersion or pouring application. Therefore, spraying was finally selected not only because of its versatility as an application technique but also because it enabled better control of the amount of treatment product applied over the sample surfaces. Prepared gel viscosities were evaluated at 25.0 ± 0.1 °C using a rheometer R/S+ (Brookfield AMETEK, Massachusetts, USA) and the software Rheo 2000 version 28.

2.5. Evaluation of Treatment Effectiveness. One month after treatment application, grazing angle (2° 2θ) XRD analyses were performed on treated sample surfaces (using the same working conditions described above) in order to investigate the recrystallization of the amorphous nanoparticles. Morphology, texture examinations, and microanalysis with energy dispersive X-ray spectroscopy (EDX) were done using a field emission scanning electron microscope (FESEM) model Auriga (Carl Zeiss SMT). Samples were carbon coated and secondary electron (SE) images were acquired by FESEM using the SE-inLens detector at an accelerating voltage of 3 kV. Additionally, cross sections of the treated samples (i.e., cut perpendicularly to the treated surface) were prepared in order to evaluate treatment penetration within the different substrates. Cross sections were carbon coated and examined using the backscatter electron detector of an environmental SEM (ESEM) model Quanta 400 (FEI). Point microanalyses and element distribution maps were performed with an EDS XFlash detector (Bruker) at an accelerating voltage of 20 kV.

To evaluate the acid resistance capacity of the samples after treatment, sample probes were immersed in 25 mL of hydrochloric acid solution with a pH of 4 at room conditions, and the pH was monitored using a Titrando 905 system (Metrohm) coupled to a pH

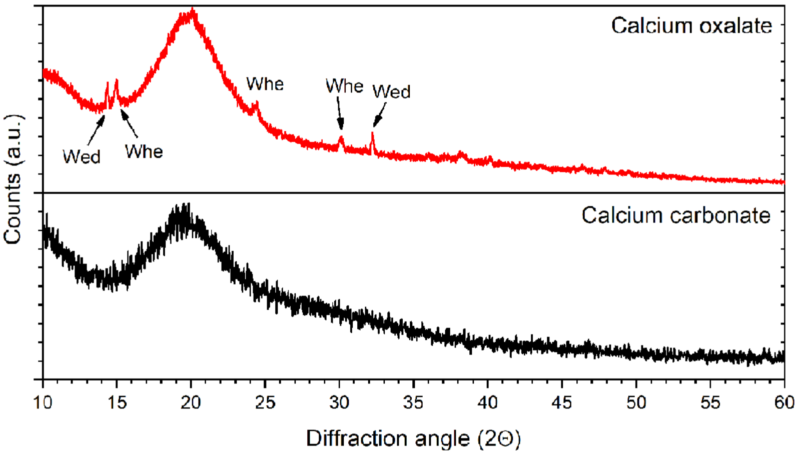

Figure 1. Powder X-ray diffraction patterns of the synthesized nanoparticles: Whe, whewellite (calcium oxalate monohydrate); Wed, weddellite (calcium oxalate dihydrate).

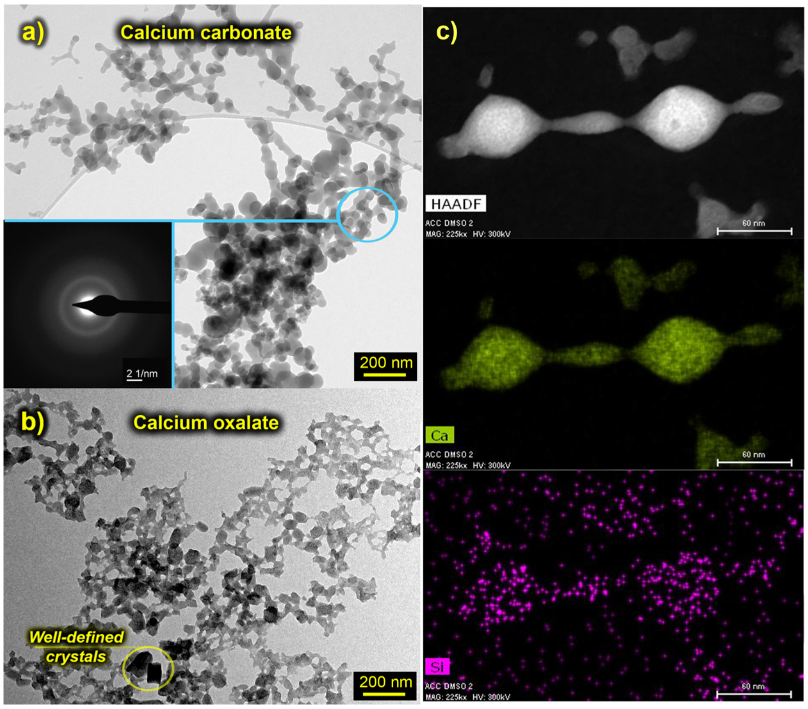

Figure 2. TEM images of the synthesized nanoparticles: (a) amorphous calcium carbonate (ACC) and corresponding SAED pattern of the blue-circled area; (b) amorphous calcium oxalate (ACO) and the corresponding SAED pattern of the blue-circled area. The yellow-circled area shows well-formed whewellite nanocrystals. (c) HAADF image and Ca-Kα and Si-Kα EDS maps of ACC nanoparticles.

meter (Electrode Plus model 6.0262.100, Metrohm) and controlled by a computer with the software Tiamo version 2.5 for continuous data log (Figure S1). pH measurements enabled us to determine the neutralization rate of the solution as a result of the dissolution of the samples' surface. After acid-attack tests, samples were carbon coated and SEM images were collected to evaluate damage.

Color changes were determined according to CIEDE2000[60] using a spectrophotometer Minolta CM-700 d, with the standard illuminant D65 and observer at 10°. Color coordinates L^* (luminosity or lightness which varies from black with a value of 0 to white with a value of 100), a^* (which varies from positives values for red to negatives values for green), and b^* (which varies from positives values for yellow to negatives values for blue) were measured. The color change ΔE^*_{ab} was calculated using the equations proposed by Sharma et al. (2005). At least 20 measurements on every sample were done before and after treatment.

Modification of the pore access size distribution upon treatment application was determined by means of mercury intrusion porosimetry (MIP) using a Micromeritics Autopore III 9410 equipment with a maximum injection pressure of 414 MPa. Three replicates per treatment (as well as untreated samples) were done. Samples with mass between 1 and 2 g were used.

The permeability to water vapor (WVP) was determined according to European Norm (EN) 15803:2010[61] using the wet cuvette method, test samples 45 mm × 45 mm × 10 mm in size, and the test device (see Figure S2) proposed by the EN. First, test samples were placed in a climatic chamber model KMF 5.2 (BINDER GmbH, Tuttlingen, Germany) at 23 °C and a relative humidity (RH) of 50% up to constant weight. Afterward, a saturated KNO_3 solution was placed inside the cuvette to maintain a constant 93% RH and the cuvette was closed with a lid that has embedded the stone/plaster slab (Figure S2). Three replicates of each sample were placed in the

DOI: 10.1021/acsanm.9b00905

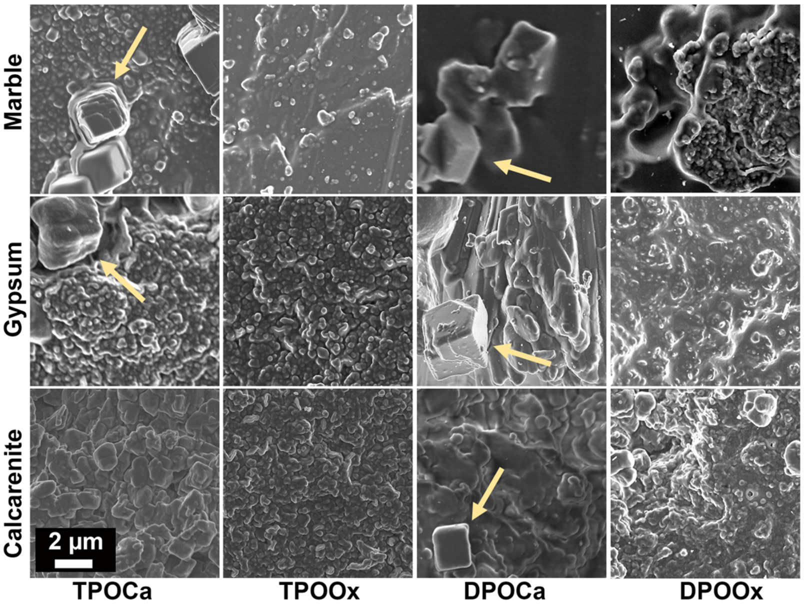

Figure 3. Representative FESEM images of the samples after treatment application. Yellow arrows show rhombohedral calcite crystals. The scale bar applies to all photomicrographs.

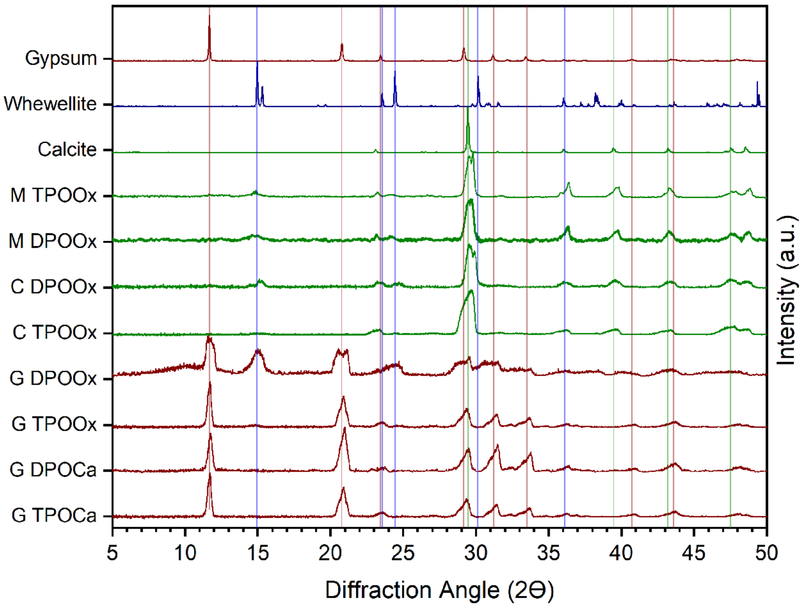

Figure 4. Grazing angle XRD patterns of samples with differences between substrate and nanoparticle composition. Color lines mark the most intense Bragg peaks of the mineral phases: green, calcite; red, gypsum; blue, whewellite. C, calcarenite; G, gypsum; M, marble.

climatic chamber at 23 °C and 50% RH, weighing the assay devices periodically for a month.

To evaluate the mechanical properties and the consolidation behavior of the applied gels on treated samples, drilling resistance tests were performed using the drilling resistance measurement system (DRMS, SINT Technology, Firenze, Italy). The 10 mm deep holes were done using a 5 mm diameter drill-bit with flat diamond head. Specific test conditions for each substrate were selected based on extensive testing aimed at disclosing optimal drilling and penetration rates for maximum signal-to-noise ratio. For marble samples, a rotation speed of 600 rpm and penetration rate of 10 mm/min were used; in the case of gypsum, a rotation speed of 200 rpm and penetration rate of 20 mm/min were selected, and for calcarenite a rotation speed of 300 rpm and penetration rate of 10 mm/min were chosen. At least six measurements per treatment and substrate type were done.

For the evaluation of the surface hydrophobicity, static contact angle measurements were done according to EN 15802:2009.[62] Water drops of 7.5 μL were deposited on the samples surface, and a picture of every drop was acquired with a Nikon D5300 digital camera before 6 s after drop deposition. Samples were placed between the camera and a light source and fixed to the vertical central point of the acquired images. Subsequent image processing for static contact angle determination was done with the software Autocad 2014. The contact angle of at least 20 drops deposited per every treatment and substrate type was determined

3. RESULTS

3.1. Characterization of Nanoparticles. Figure 1 shows that synthesized calcium carbonate nanoparticles were amorphous (ACC) as reflected by the broad hump between

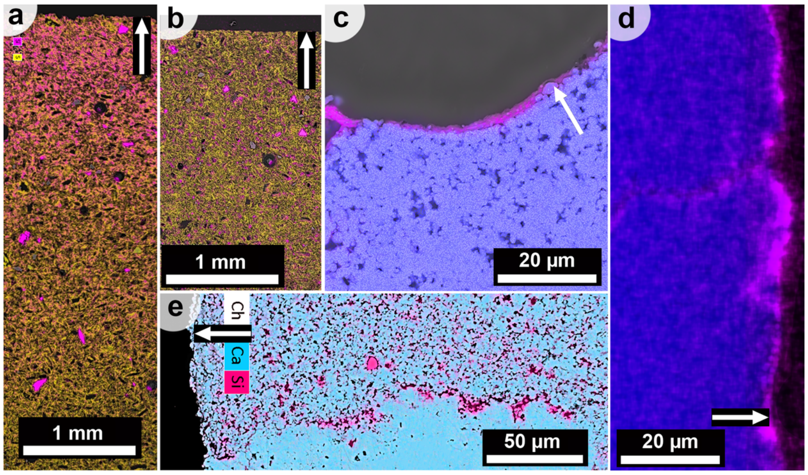

Figure 5. BSE images with element maps from selected cross sections: (a) gypsum treated with DPOCa; (b) gypsum treated with TPOCa; (c) calcarenite treated with DPOCa; (d) marble treated with DPOCa; (e) calcarenite treated with TPOCa. Color code: blue, Ca-Kα; yellow, S-Kα; pink, Si-Kα. White arrows indicate the surface of the samples.

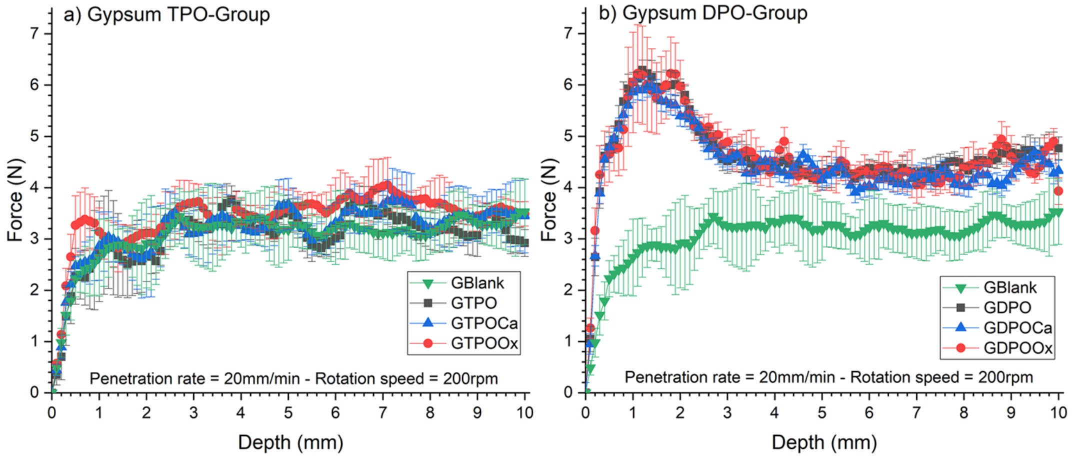

Figure 6. Drilling resistance measurements for gypsum: (a) TPO group; (b) DPO group. Error bars show $\pm 2\sigma_N$ ($N \geq 6$).

15° and 25° 2θ in the X-ray diffraction pattern[63] and the lack of diffraction peaks corresponding to any of the crystalline calcium carbonate polymorphs. In the case of calcium oxalate, it was found that most of the precipitate was amorphous (ACO) but trace amounts of calcium oxalate monohydrate (whewellite) and calcium oxalate dihydrate (weddellite) were detected. In the absence of PDMS and under our synthesis conditions, all the amorphous nanoparticles rapidly (within minutes) underwent transformation into crystalline phases as observed in previous works.[36,64] Conversely, nanoparticles synthesized in the presence of PDMS were stable for several weeks. Note that the latter ones were those used in the tested treatments.

TEM imaging (Figure 2a) showed that only ACC nanoparticles with no well-defined shape and with an average size below 100 nm formed in the calcium carbonate system. The diffuse haloes in the SAED pattern (inset in Figure 2a) confirmed the lack of crystallinity of the nanoparticles. A large amount of ACO nanoparticles with an average size of ≤50 nm formed along some well-defined crystals in the case of the calcium oxalate system (Figure 2b). In both cases, a low-contrast veil corresponding to PDMS covering the nanoparticles was observed in HAADF images (Figure 2c). EDS analysis (Figure 2c) confirmed the presence of silicon in the veil area, as well as in the bulk ACC nanoparticles.

3.2. Evaluation of Treatment Effectiveness. Figure 3 shows that in the case of the treatments containing ACC nanoparticles (i.e., TPOCa and DPOCa), ACC recrystallized to rhombohedral calcite crystals with size up to ~1 μm (see also Figure S3 and Figure S4) which left a limited number of nanoparticles present on the samples' surfaces. In the case of the treatments containing ACO nanoparticles (i.e., TPOOx and DPOOx), the size of the crystalline phases detected using grazing angle XRD analysis (whewellite, Figure 4) was smaller (between 100 and 250 nm) as compared to the treatment containing ACC nanoparticles, as seen in FESEM images (Figure 3). The morphology of the whewellite particles formed in our experiments did not match the common growth habit reported for this phase (short prisms elongated along [001]).[65] In the case of the DPO-group treatments, the gel covering the surface of the different substrates was apparently thicker than that formed in the case of the TPO-group treatments. The latter showed a more uniform surface coverage. Additionally, in the case of marble samples a very limited penetration of both TPO- and DPO-group treatments was demonstrated by BSE imaging of samples cross sections (Figure 5) and the thicker surface coatings (Figures S4 and S5).

Backscattered electron microscopy (BSE) images of cross sections (Figure 5) also showed a lower penetration depth in the case of DPO-group treatments as compared to the TPO-group treatments. In the latter case, a more homogeneous distribution of the product within the porous system of the samples was achieved (Figure 5b).

Grazing angle (2° 2θ) XRD patterns performed on samples with a contrasting mineralogical composition between the substrate and the nanoparticles showed that amorphous nanoparticles recrystallized to calcite and to whewellite, in the case of the treatment with ACC and ACO, respectively (Figure 4). Note that grazing angle XRD favors diffraction of X-rays from the surface of a sample (i.e., intact test cubes, directly analyzed with no prior grinding). Because marble and calcarenite samples include calcite, treatments with ACC nanoparticles leading to conversion into calcite showed no change in their XRD patterns. This is why they are not shown in Figure 4.

In the case of gypsum samples only, application of the treatments led to a distinct increase in dilling resistance, which was more pronounced in the case of DPO-group treatments (Figure 6b). For gypsum and within a particular treatment group (TPO or DPO group), no significant differences in drilling resistance along the depth profiles were observed (Figure 6a) except in the case of the gypsum samples treated with the DPO-group (Figure 6b). In this latter case, a significant increase in the drilling resistance along the first ~2 mm of the depth profile was observed regardless of whether they contained nanoparticles or not, which suggests that this treatment concentrated in such a near-surface area where nanoparticles present at the sample surface did not apreciably contribute to an increase in drilling resistance. Apparently, nanoparticles detached from the sample surface as soon as the drill bit touched them. Due to the larger pore size and heterogeneity of the calcarenite samples, a significant dispersion in drilling resistance values was found (Figure S6a), which precluded drawing any conclusions regarding the depth of treatment penetration or the relative increase in drilling resistance. In the case of the marble, a much higher resistance to drilling was observed[66] (Figure S6b), which together with the low penetrability of the treatments associated with its low porosity[67] made it impossible to unambiguously measure differences in drilling resistance after treatments.

Regardless of the treatment type, marble samples presented a significant color change mainly due to a decrease in the luminosity component (ΔL^*), while the changes in the Chroma component (ΔC^*) were almost negligible. Overall, this resulted in relatively high ΔE^*_{ab} values (4.5−7, Figure S7) leading to a "plastic" or "wet" appearance of the surface. In the case of TPO treatments applied on gypsum and calcarenite substrates, the color changes were negligible, with $\Delta E^*_{ab} \leq 3$.[60] Regarding DPO treatments, perceptible changes were observed when applied onto gypsum and calcarenite substrates. However, the measured changes, which varied within the range $5 \geq \Delta E^*_{ab} \geq 3$, could be catalogued as detectable by the human eye but still acceptable for conservation purposes.[68] Both gypsum and calcarenite treated with the DPO treatments group showed a reduction in the luminosity component (negative ΔL^* values), associated with a slight darkening effect of the coating, together with an increase of the color saturation given by positive ΔC^* values.[69]

The results of acid resistance tests showed a significant increase in the time required for neutralization of the hydrochloric acid solution (initial pH 4) in all treated substrates (Figure 7). Neutralization times were systematically higher in the case of all substrates treated with DPO

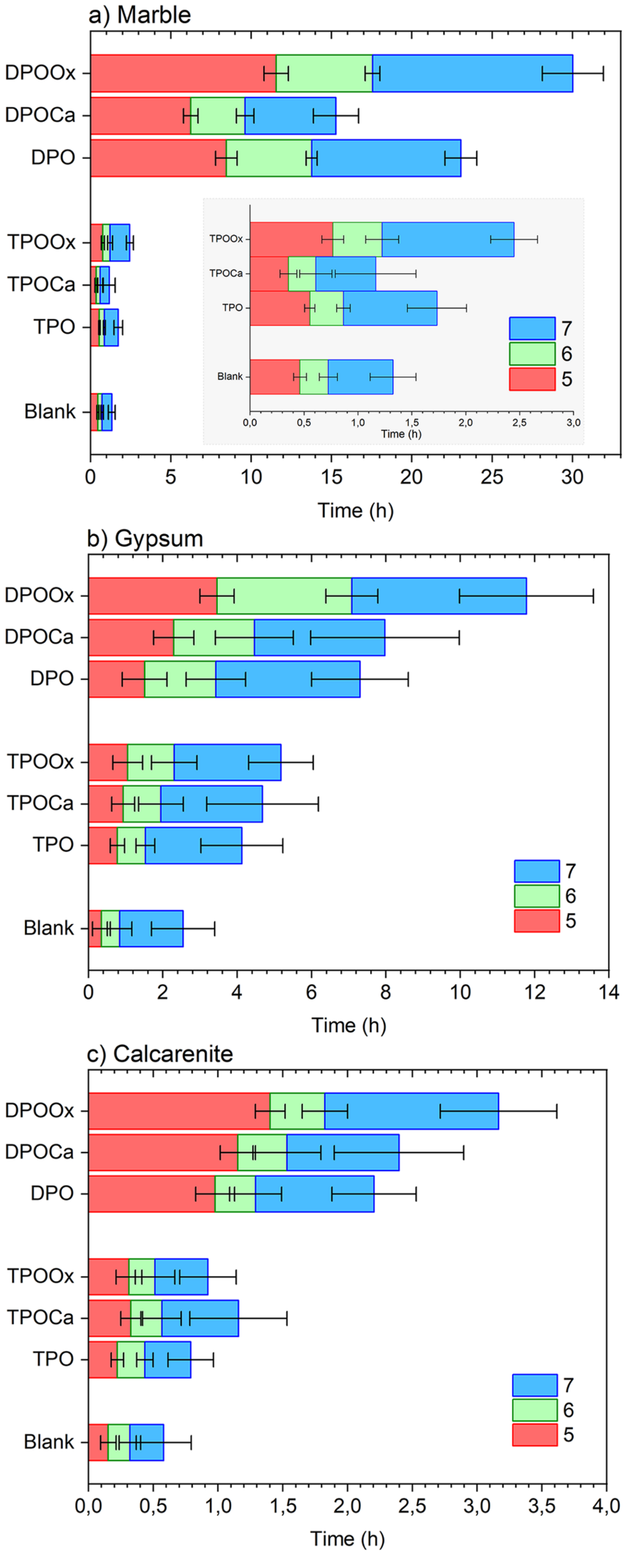

Figure 7. Required time for reaching different pH values (5, red; 6, green; 7, blue) during acid-resistance tests for (a) marble, (b) gypsum, and (c) calcarenite. Inset in (a) shows an enlarged view of the control and TPO-group treatments (t −3 h). Error bars show $\pm 2\sigma_N$.

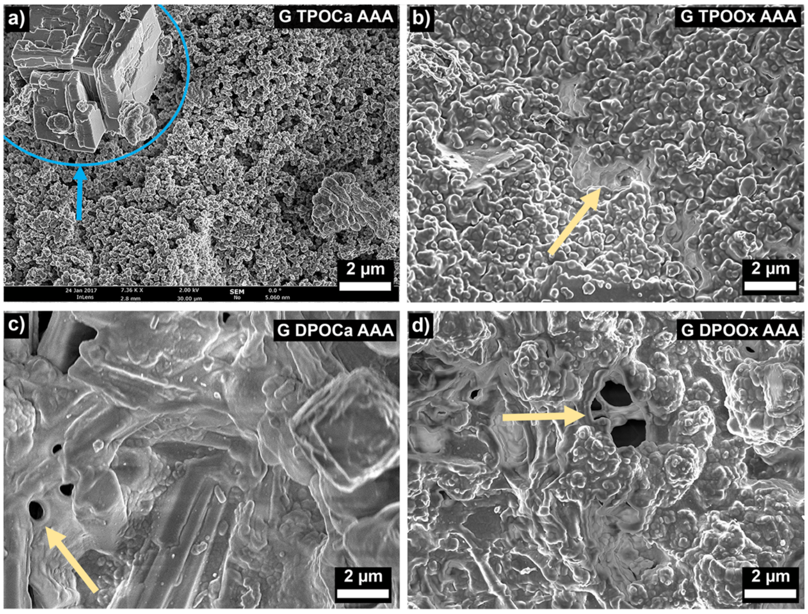

Figure 8. Selected FESEM images of gypsum treated sample surfaces after acid-attack (AAA) tests showing (a) corroded (partially dissolved) calcite (area marked by the blue circle) and general loss of the polymer gel, (b) partial surface loss of the silica gel coating which also shows crack development (yellow arrows), and (c) calcite rhombohedra still protected by the silica coating. However, cracking and holes (arrow) are observed in the gel. (d) Absence of corrosion in the substrate or in calcium oxalate and incipient development of holes in the polymer gel.

treatments compared with TPO treatments. Within the DPO group, the application of the DPOOx treatment, initially containing ACO nanoparticles, resulted in the longer times for neutralization of the acid solutions. In the case of the calcarenite and gypsum substrates, the time required to reach the different reference pH values (5, 6, and 7) was significantly longer in the case of treated samples (irrespectively of the treatment applied), as compared with untreated ones (blank). That was also the case of the marble substrate, with the exception of the samples treated with TPOCa.

FESEM images of gypsum samples subjected to the acid resistance test (Figure 8; see also Figure S8 and Figure S9) showed that the silica gel covering the surface was damaged by the acid. Shrinking of the gel as denoted by the occurrence of gel-free areas was observed, especially in the case of the DPO-group treatments. It was also observed that some of the nanoparticles were left exposed. In the case of the treatments containing ACC nanoparticles and for all substrates, dissolution of the recrystallized calcite was observed (see Figure 8a). This agrees with the lower neutralization time (see Figure 7a) for TPOCa and DPOCa treatments because calcite was easily dissolved under acidic conditions. Interestingly, marble samples treated with TPO and DPO treatments without nanoparticles and subjected to acid resistance tests showed massive cracking and shrinking (crack width of ∼200–400 μm) of the silica gel coating (Figure S9a), as well as its complete detachment in some areas which exposed the marble surface as fully pitted and corroded by the acid-promoted $CaCO_3$ dissolution (Figure S9b). These results demonstrate that there was very little adhesion between the silica coating and the marble surface. Conversely, the surface of marble treated with TPO and DPO containing nanoparticles presented small lacunae (∼10–20 μm in diameter) (Figure S9d and S10c) and narrow cracks (crack width ≤20 μm) that exposed the treatment-marble interface at their dead-end indicating limited gel shrinking (Figure S10d,e). The cracks typically displayed a wedge- or V-shaped profile (normal to the treatment surface) showing that no detachment of the treatment layer occurred at the treatment-substrate interface. Indeed, at the narrow dead-end of the cracks, the treatment was still observed to be attached to the substrate. Altogether, these results demonstrate that the nanoparticles enabled a stronger bonding of the silica gel to the non-silicate substrates and enhanced the resistance to acid attack.

In the case of the calcarenite and gypsum substrates changes in the porosity were evaluated (Figure S11) but not in the case of the marble due to its limited porosity (∼1.8%) and the lower penetrability of treatments. It was observed that both TPO- and DPO-group treatments reduced systematically the open porosity of both gypsum and calcarenite substrates. No differences were found within a particular treatment group (i.e., with and without nanoparticles). Note that nanoparticles tended to remain on the sample surfaces, therefore not contributing to a reduction in the porosity of bulk samples. In the case of the calcarenite, the amount of coarse pores (i.e., $r > 1$ μm) decreased while the amount of small pores (i.e., $r < 1$ μm) increased. The latter is in agreement with the silicon maps of cross sections where a partial filling of pore spaces by silicon was observed (Figure 5). The largest reduction in the amount of coarse pores was observed in the TPO-group treatments. In the case of gypsum substrates, TPO-group treatments led to a slight reduction in the volume of coarse pores while DPO-group treatments induced a reduction in the volume of pores with size $0.01 < r < 0.1$ μm. Changes in the internal porosity of any material due to filling of empty spaces typically lead to an increase in its mechanical strength but also to a reduction in its permeability. The latter may in turn lead to undesirable effects related to impermeabilization toward gases. However, in the case of the marble and calcarenite substrates, no significant changes were found in the water vapor permeability, WVP (Figure S12). Only in the case of gypsum samples a slight reduction in WVP from 0.013 ± 0.005 g/(m^2 h Pa) in the untreated samples to ∼0.012 g/(m^2 h Pa) in both the TPO- and DPO-group treatments was observed (Figure S12).

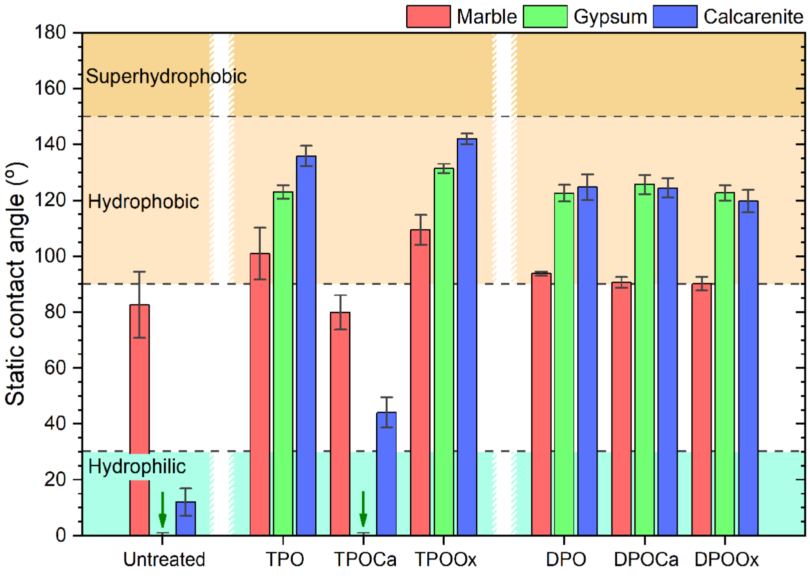

Figure 9. Static contact angles of treated and untreated samples. Error bars show $2\sigma_N$.

However, such a reduction in WVP was within error of the measurements.

All treatments could be regarded as hydrophobic as deduced from the measured static contact angles of the different substrates after treatment application (Figure 9). Regardless of the substrate type, the highest static contact angles were obtained following TPOOx treatment. However, in the case of TPOCa treatments, nonhydrophobic contact angles were obtained. On the contrary, in the case of DPO treatments, hydrophobic contact angles were obtained systematically, but no significant differences in contact angle between nanoparticle-free and nanoparticle-inclusive treatments were observed.

4. DISCUSSION

Our results show that nanoparticles synthesized by mixing Ca^{2+} and CO_3^{2-} or $C_2O_4^{2-}$ emulsions, using PDMS as emulsifying agent, lead to stable ACC and ACO nanoparticles, respectively, with an average size below 100 nm (Figure 2). The use of PDMS as emulsifying agent also makes the amorphous nanoparticles suitable to be integrated in the hybrid matrix of the gel during the sol–gel transition of the alkoxysilane treatments used here. This should be fostered by the fact that the nanoparticles are covered by PDMS, as demonstrated by our HAADF-EDS analyses. Such a surface layer would enable a direct bonding with the silica gel matrix. Moreover, our results suggest that PDMS was pivotal for a lasting and effective stabilization of amorphous phases, which enables application of the nanoparticle-based treatments in their original (amorphous) state. PDMS is an elastomer whose presence in TEOS-based polymers influences not only the chemical properties of the coatings (making them more elastic[70−72]) but also their surface morphology and hydrophobic character favoring a dual-scale roughness which enhances the hydrophobic behavior of Si coatings.[11−14,73,74] Among the advantages of using PDMS, it has been shown that some PDMS compounds as the one selected here with hydroxyl-terminated functional groups can also act as coupling agents between the gel network and non-silicate substrates.[12] Ultimately, PDMS facilitates condensation reactions in the sol–gel process and is perfectly integrated into the inorganic gels network,[28] and due to its low surface energy, it reduces the pore size of the gel network. The latter effects result in a reduction of gel-cracking that also provides toughness and flexibility. It has also been reported that nanoparticles contained in gels, together with surfactants (e.g., *n*-octylamine), prevent gel-cracking during drying and/or curing.[12] This is why *n*-octylamine was also used here to prevent gel cracking by acting as a template during the formation of the gel network and as a basis catalyst.[28,75]

All these positive effects brought about by the amorphous nanoparticles in combination with PDMS and *n*-octylamine are in good agreement with our results as rough surfaces (Figure 3), increased static contact angles (Figure 9), and the absence of cracks in the gel layer were obtained. These results are comparable but superior to those obtained by Manoudis and co-workers[16] using TEOS dosed with SiO_2 nanoparticles. Taking 90° as the threshold contact angle considered as minimum for stone protection,[76] all the tested treatments, with the exception of TPOCa, could be considered as effective hydrophobicing agents for stone protection. In particular, TPOOx treatments displayed a significant increase in the values of static contact angle for all substrates as compared with reference TPO treatments (i.e., without nanoparticles). Conversely, DPO-group treatments with and without nanoparticles showed similar static contact angles (within error). This is likely due to the fact that DPO treatments prevented the development of surface rugosity (vide infra). Overall, the higher static contact angles of TPO-group treatments could be attributed to the lower viscosity of this treatment that facilitates the product distribution along sample surfaces, ultimately resulting in a higher micro- and nanorugosity of the surface. This is in agreement with the hierarchical surface topography observed in SEM (Figure 3). In the particular case of the TPOCa treatment, ACC nanoparticles used in the initial TPOCa dispersion resulted in a final homogeneous distribution of partially gel-embedded rhombohedral calcite crystals with an average size of ∼1 μm. ACC transforms into calcite via dissolution−precipitation, likely fostered by the presence of water in the initial solution sprayed onto the surfaces and/or moisture from the environment. Such a microstructure prevented the development of a Casey regime, and being such crystals hydrophilic, they also increased the wettability of the treated substrate. In this case, and for the different tested substrates, these calcite crystals acted as sacrificial material during acid weathering as observed using FESEM (Figure 8) and in agreement with the lower neutralization times observed during the acid-attack test (Figure 7). However, a poor hydrophobicity was achieved. This is not necessarily a negative or undesirable phenomenon in terms of stone protection. Those rhombohedral calcite crystals will dissolve before any other material from the substrate surface behind the gel and therefore will protect the original surface against dissolution. In the case of DPOCa treatments and despite the fact that some calcite crystals were also present, the hydrophobic contact angles measured could be attributed to the greater thickness of treatment product remaining on the sample surfaces. However, such a higher amount of silica gel with embedded amorphous ACC or ACO (or their crystalline product) smoothed the surface, thereby preventing the development of a Wenzel and Cassie−Baxter regime.[19−21] As a result, the contact angles were lower than those achieved with the less viscous TPO-group treatments (with the exception of TPOCa, as indicated above). A rougher initial surface in the case of the very porous gypsum plaster and the calcarenite substrates also explain why their contact angles after TPO-group treatment application were systematically higher (again, with the exception of TPOCa) than those measured in the case of the smooth (nonporous) treated marble surface.

Conversely, it is also known that nanoparticles may affect the aesthetic appearance of surfaces, as also occurs with many other surface treatments.[2,77,78] In general, the higher the nanoparticle concentration is, the greater its aesthetic effect would be.[30] However, in our case, the foregoing effect was within acceptable values for conservation purposes.[68] Indeed, color differences between treatments with and without nanoparticles were within error (Figure S7). Nonetheless, the colorimetric results indicate that, in general, both TPO- and DPO-group treatments are suitable for the conservation of porous substrates. Results from colorimetric measurements seem to be related to differences in viscosity of treatment products, which play an important role in the penetrability of the products within the porous substrates. Results from elements distribution performed with the EDS detector on BSE images of cross sections (Figure 5a) suggest that the higher is the viscosity of the treatment product, the more limited is the penetration depth. A higher viscosity (3.7 ± 0.5 mPa·s), and, hence, lower penetrability of the product, in the case of the DPO-group treatment resulted in ∼2 mm thick Si-rich surface rim, as was clearly observed in the case of the gypsum samples (Figure 5a). The latter explains the higher drilling resistance (Figure 6b, DPO-group) found along the first ∼2 mm along the depth profile of treated gypsum samples. In the case of the calcarenite and due to its heterogeneous nature and pore size distribution, the DPO-group treatments penetrated in a more uniform way as shown by the element distribution maps of BSE images (Figure 5c,e). However, in this latter case (calcarenite samples), the higher viscosity of DPO-group treatments resulted in localized product accumulation within the cavities and holes of the calcarenite, where a silicon-rich rim with an average thickness of ∼1 μm was observed (Figure 5c,e). Such an accumulation of the treatment product was likely responsible for the observed greater aesthetic differences (i.e., higher ΔE^*_{ab} values). In the case of the TPO-group treatments, which presented a lower viscosity (1.2 ± 0.2 mPa·s), a more homogeneous distribution of the product within the porous system of the samples was achieved. Indeed, the largest reduction in the amount of coarse pores in porous samples after treatment with TPO group can be also related to a more homogeneous distribution of the treatment within the porous substrate due to the lower viscosity of these treatments as compared with the DPO group. In the case of marble, the limited penetrability of both types of treatments was not unexpected due to its very low porosity. For gypsum samples, the higher treatment penetration can explain the significant strengthening effect observed, as shown by the increased drilling resistance measured here. The limited differences found within a particular treatment group could be attributed to the presence of ACC or ACO nanoparticles within the bulk substrate, as they tended to accumulate on the first μm of the sample depth. In the case of the marble, the very high drilling resistance of the substrate and the negligible penetration of the treatments prevented any significant strengthening effect of the different treatments from drilling resistance measurements (Figure S6b). In the case of the calcarenite, the heterogeneous nature of this stone and the high dispersion in the values of drilling resistance also prevented any possible strengthening effect of the different treatments (Figure S6a).

The resistance against acid attack following treatment was related to the type of nanoparticles used. ACO nanoparticles led to a drastic increase in the resistance against acid attack, regardless the type of treatment group (i.e., TPOOx or DPOOx). The highest required times for neutralization of the acid solutions obtained for the DPOOx treatment (Figure 7) are attributed to two main effects: (i) the limited wettability of the surface because of the hydrophobic character of the treatment and (ii) the presence of a less soluble phase (i.e., calcium oxalate) within the surface coating that may also act as a protective layer when the substrate is subjected to dissolution. In contrast, the use of relatively soluble ACC nanoparticles (and the calcite crystals resulting from the amorphous-to-crystalline phase transformation) provided the same resistance against acid attack (within error) as that of treatments without nanoparticles. In the case of the marble, shorter neutralization times were observed for both TPOCa and DPOCa treatments which could be attributed to the higher amount of precipitated micrometer-sized calcite aggregates (formed after ACC) on the surface. This is likely due to the low penetrability of the treatments, leading to a surface accumulation of ACC (or calcite) that could be easily dissolved thereby acting as a sacrificial material.

Acid tests also disclosed that the presence of nanoparticles, especially ACO-containing treatments applied on marble, significantly reduced loss of surface silica gel coating and its cracking and shrinking (Figures S9 and S10). In the presence of nanoparticles, micrometer-sized holes and narrow cracks with a V-shaped cross-sectional profile developed after acid attack, but they did not affected the full treatment profile. Indeed, our FESEM observations showed that the treatment was still attached to the substrate at both the bottom of holes/lacunae and cracks. Apparently, the nanoparticles limited treatment loss, cracking, and shrinking because they enabled a stronger bonding between the non-silicate substrate and the alkoxysilane-based treatment. Chemical bonding between gel components and nanoparticles in our study can be inferred from FTIR. Figure S13 shows spectra of individual gel components and the gels containing both calcium carbonate and calcium oxalate amorphous nanoparticles. A shift can be observed from the band corresponding to Si−OH bonds, from 1620 to 1640 cm^{-1} that could reflect the interaction between ACO and ACC nanoparticles and PDMS. The 860 cm^{-1} band in PDMS is also shifted due to bonding with nanoparticles within the gel. Moreover, in the case of treatment with ACC nanoparticles, the calcite peak at 875 cm^{-1} corresponding to out-of-the-plane C−O bending shows a shift to ∼850 cm^{-1} that suggests a reaction among Si−O−Si and carbonate groups.

Likely, this was due to an epitaxial crystallization of calcium carbonate or calcium oxalate crystals (formed after the amorphous nanoparticles) on the treated substrates, enabling crystallographic continuity and a strong bonding between the substrate and the treatment layer as schematically depicted in Figure S10f. Note that an obvious epitaxy, or more exactly, self-epitaxy, exists between calcite (present in both the tested marble and calcarenite) and calcite formed after ACC, as both have the same crystal structure. Calcium oxalates have also been shown to grow epitaxially on calcite crystals.[2,44,45] Moreover, calcite (formed after ACC) and gypsum have been shown to display an epitaxial relationship.[43,79] Finally, it is worth mentioning that despite the fact that hydroxyl-terminated PDMS could enable the bonding between the silica gel treatment and the calcitic and gypsum substrates, such a bonding does not seem to be very strong or durable, as suggested by the extensive cracking, shrinking, and massive detachment of the silica gel coating in samples treated with TPO and DPO treatments without nanoparticles and subjected to acid attack (Figure S10a and Figure S10f).

Consequently and considering the trade-off between the use of different types of nanoparticles and additives which help to balance a compromise between a maximum water repellency, crack prevention, strengthening of the bonding between the applied gels and the substrates, treatment durability, (acid) weathering resistance, and minimum aesthetic impact, both TPO and DPO treatments with ACO nanoparticles could be considered optimal for conservation purposes. Nonetheless, treatments containing ACC nanoparticles should not be discarded because of their relatively high solubility and preferential dissolution during the action of weathering agents (e.g., acid solutions or rainwater), as such a sacrificial effect will help protect and preserve the substrate underneath. They will also be optimal to ensure a good bonding between the marble or limestone calcitic substrate and the silica gel.

In any case, both ACC and ACO will eventually transform into crystalline phases with a lower molar volume. This enables the generation of porosity, especially within the surface coating formed on top of the treated substrates. The latter can help reduce one of the main drawbacks of the use of alkoxysilanes in stone conservation: i.e., the formation of impervious layers. Here, we show that indeed the reduction in water vapor permeability 2 months after treatment application, when calcite and weddellite have formed after ACC and ACO, respectively, is negligible. Moreover, the formation of both crystalline $CaCO_3$ (calcite rhombohedra) and $CaC_2O_4 \cdot H_2O$ (whewellite) did not result in any detrimental effect on the integrity of the silica gel coating. Indeed, their formation led to no detrimental effect during acid resistance tests. Actually, a significant improvement in the silica gel acid resistance as compared with reference treatments without nanoparticles was observed (Figure 7 and Figures S8−S10).

ACC and ACO nanoparticles thus provide an effective bioinspired solution for overcoming the main drawbacks of the use of alkoxisilanes in stone conservation.

5. CONCLUSIONS

Our results show that the bioinspired approach based on the use of amorphous nanoparticles in combination with alkoxysilane-based gels could be suitable for the protection of the aforementioned type of stone or plaster materials. It has been found that the viscosity of the initial sprayed solutions has a marked influence on the strengthening and protective effects of the treatments. The higher the initial viscosity of the solution is, the greater the consolidation and protective effect of the product are but the less homogeneous the distribution of the treatment is along the samples' depth profile and the higher the color changes are. The applied nanoparticles contributed to overcome the main drawback of alkoxysilanes: gel cracking during drying and curing while enhancing the hydrophobic behavior of the coating due to the transition from a Young−Laplace to a Wenzel and Cassie−Baxter regime due to the observed changes in surface topography. Moreover, amorphous nanoparticles, especially calcium oxalate ones, confer an enhanced acid resistance (∼45%) to the applied treatments, presenting limited impact on aesthetic and hydric properties. Addition of the nanoparticles fostered the bond of the alkoxysilane treatment to non-silicate substrates, especially in the case of the marble. This was likely due to an epitaxial crystallization on the substrates of calcium carbonate or calcium oxalate crystals (formed after the amorphous nanoparticles) that enabled the anchoring to the substrate of the silica gel formed upon alkoxysilane sol−gel transition.

■ ASSOCIATED CONTENT

Ⓢ Supporting Information

The Supporting Information is available free of charge on the ACS Publications website at DOI: 10.1021/acsanm.9b00905.

Figures S1−S13 (PDF)

■ AUTHOR INFORMATION

Corresponding Author

*E-mail: encaruiz@ugr.es.

ORCID

A. Burgos-Cara: 0000-0001-7268-0664
C. Rodríguez-Navarro: 0000-0002-3179-8428
M. Ortega-Huertas: 0000-0002-8958-1061
E. Ruiz-Agudo: 0000-0003-1292-4000

Notes

The authors declare no competing financial interest.

■ ACKNOWLEDGMENTS

The authors acknowledge funding from European Commission (European Regional Development Fund, Grant CGL2015-70642-R), Junta de Andalucía (Grant P11-RNM-7550, Research Group RNM-179), Ministerio de Economía y Competitividad (Grants CGL2015-70642-R, CGL2015-73103-EXP), and Universidad de Granada (Grant UCE-PP2016-05).

■ REFERENCES

(1) Doehne, E.; Price, C. A. *Stone Conservation: An Overview of Current Research*; Getty Conservation Institute: Los Angeles, CA, 2011.

(2) Burgos-Cara, A.; Ruiz-Agudo, E.; Rodriguez-Navarro, C. Effectiveness of Oxalic Acid Treatments for the Protection of Marble Surfaces. *Mater. Des.* **2017**, *115*, 82−92.

(3) Daniele, V.; Taglieri, G.; Quaresima, R. The Nanolimes in Cultural Heritage Conservation: Characterisation and Analysis of the Carbonatation Process. *J. Cult. Herit.* **2008**, *9* (3), 294−301.

(4) Graziani, G.; Sassoni, E.; Franzoni, E. Consolidation of Porous Carbonate Stones by an Innovative Phosphate Treatment: Mechanical Strengthening and Physical-Microstructural Compatibility in Comparison with TEOS-Based Treatments. *Heritage Sci.* **2015**, *3*, 1.

(5) Sassoni, E.; Franzoni, E.; Pigino, B.; Scherer, G. W.; Naidu, S. Consolidation of Calcareous and Siliceous Sandstones by Hydroxyapatite: Comparison with a TEOS-Based Consolidant. *J. Cult. Heritage* **2013**, *14* (3, Suppl.), e103−e108.

(6) Ciardelli, F.; Aglietto, M.; Montagnini di Mirabello, L.; Passaglia, E.; Giancristoforo, S.; Castelvetro, V.; Ruggeri, G. New Fluorinated Acrylic Polymers for Improving Weatherability of Building Stone Materials. *Prog. Org. Coat.* **1997**, *32* (1−4), 43−50.

(7) Salazar-Hernández, C.; Cervantes, J.; Puy-Alquiza, M. J.; Miranda, R. Conservation of Building Materials of Historic Monuments Using a Hybrid Formulation. *J. Cult. Heritage* **2015**, *16*, 185−191.

(8) Kapridaki, C.; Maravelaki-Kalaitzaki, P. TiO2-SiO2-PDMS Nano-Composite Hydrophobic Coating with Self-Cleaning Properties for Marble Protection. *Prog. Org. Coat.* **2013**, *76* (2−3), 400−410.

(9) Wheeler, G. *Alkoxysilanes and the Consolidation of Stone*; Getty Conservation Institute: Los Angeles, CA, 2005.

(10) Sena da Fonseca, B.; Ferreira Pinto, A. P.; Piçarra, S.; Montemor, M. de F. Challenges of Alkoxysilane-Based Consolidants for Carbonate Stones: From Neat TEOS to Multipurpose Hybrid Nanomaterials. *Adv. Mater. Conserv. Stone* **2018**, 185−207.

(11) Illescas, J. F.; Mosquera, M. J. Surfactant-Synthesized PDMS/Silica Nanomaterials Improve Robustness and Stain Resistance of Carbonate Stone. *J. Phys. Chem. C* **2011**, *115* (30), 14624−14634.

(12) Li, D.; Xu, F.; Liu, Z.; Zhu, J.; Zhang, Q.; Shao, L. The Effect of Adding PDMS-OH and Silica Nanoparticles on Sol-Gel Properties and Effectiveness in Stone Protection. *Appl. Surf. Sci.* **2013**, *266*, 368−374.

(13) Wu, Y. L.; Chen, Z.; Zeng, X. T. Nanoscale Morphology for High Hydrophobicity of a Hard Sol-Gel Thin Film. *Appl. Surf. Sci.* **2008**, *254* (21), 6952−6958.

(14) Mosquera, M. J.; De Los Santos, D. M.; Rivas, T. Surfactant-Synthesized Ormosils with Application to Stone Restoration. *Langmuir* **2010**, *26* (9), 6737−6745.

(15) Mosquera, M. J.; de los Santos, D. M.; Valdez-Castro, L.; Esquivias, L. New Route for Producing Crack-Free Xerogels: Obtaining Uniform Pore Size. *J. Non-Cryst. Solids* **2008**, *354* (2−9), 645−650.

(16) Manoudis, P. N.; Tsakalof, A.; Karapanagiotis, I.; Zuburtikudis, I.; Panayiotou, C. Fabrication of Super-Hydrophobic Surfaces for Enhanced Stone Protection. *Surf. Coat. Technol.* **2009**, *203* (10−11), 1322−1328.

(17) Nosonovsky, M.; Bhushan, B. Patterned Nonadhesive Surfaces: Superhydrophobicity and Wetting Regime Transitions †. *Langmuir* **2008**, *24* (4), 1525−1533.

(18) Simpson, J. T.; Hunter, S. R.; Aytug, T. Superhydrophobic Materials and Coatings: A Review. *Rep. Prog. Phys.* **2015**, *78* (8), No. 086501.

(19) Yüce, M. Y.; Demirel, A. L. The Effect of Nanoparticles on the Surface Hydrophobicity of Polystyrene. *Eur. Phys. J. B* **2008**, *64* (3−4), 493−497.

(20) Yoshimitsu, Z.; Nakajima, A.; Watanabe, T.; Hashimoto, K. Effects of Surface Structure on the Hydrophobicity and Sliding Behavior of Water Droplets. *Langmuir* **2002**, *18* (15), 5818−5822.

(21) Gao, L.; McCarthy, T. J. Wetting 101° †. *Langmuir* **2009**, *25* (24), 14105−14115.

(22) Gao, L.; McCarthy, T. J. "Artificial Lotus Leaf" Prepared Using a 1945 Patent and a Commercial Textile. *Langmuir* **2006**, *22* (14), 5998−6000.

(23) Gao, X.; Yan, X.; Yao, X.; Xu, L.; Zhang, K.; Zhang, J.; Yang, B.; Jiang, L. The Dry-Style Antifogging Properties of Mosquito Compound Eyes and Artificial Analogues Prepared by Soft Lithography. *Adv. Mater.* **2007**, *19* (17), 2213−2217.

(24) Pinho, L.; Mosquera, M. J. Photocatalytic Activity of TiO2-SiO2 Nanocomposites Applied to Buildings: Influence of Particle Size and Loading. *Appl. Catal., B* **2013**, *134−135*, 205−221.

(25) Pinho, L.; Mosquera, M. J. Titania-Silica Nanocomposite Photocatalysts with Application in Stone Self-Cleaning. *J. Phys. Chem. C* **2011**, *115* (46), 22851−22862.

(26) De Ferri, L.; Lottici, P. P.; Lorenzi, A.; Montenero, A.; Salvioli-Mariani, E. Study of Silica Nanoparticles - Polysiloxane Hydrophobic Treatments for Stone-Based Monument Protection. *J. Cult. Herit.* **2011**, *12* (4), 356−363.

(27) Xu, L.; Karunakaran, R. G.; Guo, J.; Yang, S. Transparent, Superhydrophobic Surfaces from One-Step Spin Coating of Hydrophobic Nanoparticles. *ACS Appl. Mater. Interfaces* **2012**, *4* (2), 1118−1125.

(28) Facio, D. S.; Mosquera, M. J. Simple Strategy for Producing Superhydrophobic Nanocomposite Coatings in Situ on a Building Substrate. *ACS Appl. Mater. Interfaces* **2013**, *5* (15), 7517−7526.

(29) Karapanagiotis, I.; Manoudis, P. N.; Savva, A.; Panayiotou, C. Superhydrophobic Polymer-Particle Composite Films Produced Using Various Particle Sizes. *Surf. Interface Anal.* **2012**, *44* (7), 870−875.

(30) Manoudis, P. N.; Karapanagiotis, I.; Tsakalof, A.; Zuburtikudis, I.; Kolinkeová, B.; Panayiotou, C. Superhydrophobic Films for the Protection of Outdoor Cultural Heritage Assets. *Appl. Phys. A: Mater. Sci. Process.* **2009**, *97* (2), 351−360.

(31) Verganelaki, A.; Kapridaki, C.; Maravelaki-Kalaitzaki, P. Modified Tetraethoxysilane with Nanocalcium Oxalate in One-Pot Synthesis for Protection of Building Materials. *Ind. Eng. Chem. Res.* **2015**, *54* (29), 7195−7206.

(32) Verganelaki, A.; Maravelaki, N.; Kilikoglou, V.; Karatasios, I. *Built Heritage: Monitoring Conservation Management*; Springer: Cham, Switzerland, 2015; pp 391−402, DOI: 10.1007/978-3-319-08533-3.

(33) Estroff, L. A. Introduction: Biomineralization. *Chem. Rev.* **2008**, *108* (11), 4329−4331.

(34) Gower, L. B. Biomimetic Model Systems for Investigating the Amorphous Precursor Pathway and Its Role in Biomineralization. *Chem. Rev.* **2008**, *108* (11), 4551−4627.

(35) Meldrum, F. C.; Cölfen, H. Controlling Mineral Morphologies and Structures in Biological and Synthetic Systems. *Chem. Rev.* **2008**, *108* (11), 4332−4432.

(36) Rodriguez-Navarro, C.; Burgos Cara, A.; Elert, K.; Putnis, C. V.; Ruiz-Agudo, E. Direct Nanoscale Imaging Reveals the Growth of Calcite Crystals via Amorphous Nanoparticles. *Cryst. Growth Des.* **2016**, *16* (4), 1850−1860.

(37) De Yoreo, J. J.; Gilbert, P. U. P. A.; Sommerdijk, N. A. J. M.; Penn, R. L.; Whitelam, S.; Joester, D.; Zhang, H.; Rimer, J. D.; Navrotsky, A.; Banfield, J. Crystallization by Particle Attachment in Synthetic, Biogenic, and Geologic Environments. *Science (Washington, DC, U. S.)* **2015**, *349* (6247), aaa6760−aaa6760.

(38) Rodríguez-Navarro, C.; Ruiz-Agudo, E.; Harris, J.; Wolf, S. E. Nonclassical Crystallization in Vivo et in Vitro (II): Nanogranular Features in Biomimetic Minerals Disclose a General Colloid-Mediated Crystal Growth Mechanism. *J. Struct. Biol.* **2016**, *196* (2), 260−287.

(39) Wolf, S. E.; Böhm, C. F.; Harris, J.; Demmert, B.; Jacob, D. E.; Mondeshki, M.; Ruiz-Agudo, E.; Rodríguez-Navarro, C. Nonclassical Crystallization in Vivo et in Vitro (I): Process-Structure-Property Relationships of Nanogranular Biominerals. *J. Struct. Biol.* **2016**, *196* (2), 244−259.

(40) Price, C. A. The Consolidation of Limestone Using a Lime Poultice and Limewater. *Stud. Conserv.* **1984**, *29* (sup1), 160−162.

(41) D'Armada, P.; Hirst, E. Nano-Lime for Consolidation of Plaster and Stone. *J. Archit. Conserv.* **2012**, *18* (1), 63−80.

(42) Demény, A.; Németh, P.; Czuppon, G.; Leél-Őssy, S.; Szabó, M.; Judik, K.; Németh, T.; Stieber, J. Formation of Amorphous Calcium Carbonate in Caves and Its Implications for Speleothem Research. *Sci. Rep.* **2016**, *6*, 39602.

(43) Ruiz-Agudo, E.; Putnis, C. V.; Hövelmann, J.; Álvarez-Lloret, P.; Ibáñez-Velasco, A.; Putnis, A. Experimental Study of the Replacement of Calcite by Calcium Sulphates. *Geochim. Cosmochim. Acta* **2015**, *156*, 75−93.

(44) King, H. E.; Mattner, D. C.; Plümper, O.; Geisler, T.; Putnis, A. Forming Cohesive Calcium Oxalate Layers on Marble Surfaces for Stone Conservation. *Cryst. Growth Des.* **2014**, *14* (8), 3910−3917.

(45) Ruiz-Agudo, E.; Álvarez-Lloret, P.; Putnis, C. V.; Rodriguez-Navarro, A. B.; Putnis, A. Influence of Chemical and Structural Factors on the Calcite−calcium Oxalate Transformation. *CrystEngComm* **2013**, *15* (46), 9968.

(46) Pai, R. K.; Pillai, S. Nanoparticles of Amorphous Calcium Carbonate by Miniemulsion: Synthesis and Mechanism. *CrystEngComm* **2008**, *10* (7), 865.

(47) Gehl, A.; Dietzsch, M.; Mondeshki, M.; Bach, S.; Häger, T.; Panthöfer, M.; Barton, B.; Kolb, U.; Tremel, W. Anhydrous Amorphous Calcium Oxalate Nanoparticles from Ionic Liquids: Stable Crystallization Intermediates in the Formation of Whewellite. *Chem. - Eur. J.* **2015**, *21* (50), 18192−18201.

(48) Mantilaka, M.; Rajapakse, R.; Karunaratne, D.; Pitawala, H. Preparation of Amorphous Calcium Carbonate Nanoparticles from Impure Dolomitic Marble with the Aid of Poly(Acrylic Acid) as a Stabilizer. *Adv. Powder Technol.* **2014**, *25* (2), 591−598.

(49) Hopwood, J. D.; Mann, S. Synthesis of Barium Sulfate Nanoparticles and Nanofilaments in Reverse Micelles and Microemulsions. *Chem. Mater.* **1997**, *9* (8), 1819−1828.

(50) Fricke, M.; Sundmacher, K. Emulsion-Assisted Nanoparticle Precipitation: Time Scale Analysis and Dynamic Simulation. *Ind. Eng. Chem. Res.* **2012**, *51* (4), 1579−1591.

(51) Sand, K. K.; Rodriguez-Blanco, J. D.; Makovicky, E.; Benning, L. G.; Stipp, S. L. S. Crystallization of CaCO 3 in Water−Alcohol Mixtures: Spherulitic Growth, Polymorph Stabilization, and Morphology Change. *Cryst. Growth Des.* **2012**, *12* (2), 842−853.

(52) Rodriguez-Navarro, C.; Burgos Cara, A.; Elert, K.; Putnis, C. V.; Ruiz-Agudo, E. Direct Nanoscale Imaging Reveals the Growth of Calcite Crystals via Amorphous Nanoparticles. *Cryst. Growth Des.* **2016**, *16* (4), 1850−1860.

(53) Illescas, J. F.; Mosquera, M. J. Producing Surfactant-Synthesized Nanomaterials In Situ on a Building Substrate, without Volatile Organic Compounds. *ACS Appl. Mater. Interfaces* **2012**, *4* (8), 4259−4269.

(54) Kapridaki, C.; Maravelaki-Kalaitzaki, P. TiO2-SiO2-PDMS Nano-Composite Hydrophobic Coating with Self-Cleaning Properties for Marble Protection. *Prog. Org. Coat.* **2013**, *76* (2−3), 400−410.

(55) Bello, M. A.; Martin, L.; Martin, A. Microchemical Identification of Macael White Marble in Some Spanish Monuments. *Mater. Constr.* **1992**, *42* (225), 23−30.

(56) Luque, A.; Cultrone, G.; Mosch, S.; Siegesmund, S.; Sebastian, E.; Leiss, B. Anisotropic Behaviour of White Macael Marble Used in the Alhambra of Granada (Spain). *Eng. Geol.* **2010**, *115* (3−4), 209−216.

(57) Urosevic, M.; Sebastián Pardo, E.; Ruiz-Agudo, E.; Cardell, C. Evaluación de Las Propiedades Físicas de Dos Rocas Carbonáticas Usadas Como Material de Construcción Actual e Histórico En Andalucía Oriental, España. *Mater. Constr.* **2011**, *61* (301), 93−114.

(58) Molina, E.; Cultrone, G.; Sebastián, E.; Alonso, F. J.; Carrizo, L.; Gisbert, J.; Buj, O. The Pore System of Sedimentary Rocks as a Key Factor in the Durability of Building Materials. *Eng. Geol.* **2011**, *118* (3−4), 110−121.

(59) Dominguez-Vidal, A.; De La Torre-López, M. J.; Campos-Suñol, M. J.; Rubio-Domene, R.; Ayora-Cañada, M. J. Decorated Plasterwork in the Alhambra Investigated by Raman Spectroscopy: Comparative Field and Laboratory Study. *J. Raman Spectrosc.* **2014**, *45* (11−12), 1006−1012.

(60) Sharma, G.; Wu, W.; Dalal, E. N. The CIEDE2000 Color-Difference Formula: Implementation Notes, Supplementary Test Data, and Mathematical Observations. *Color Res. Appl.* **2005**, *30* (1), 21−30.

(61) AENOR. *Conservation of Cultural Property. Test Methods. Determination of Water Vapour Permeability*; UNE-EN 15803:2010; AENOR: Madrid, 2010.

(62) AENOR. *Conservation of Cultural Property. Test Methods. Determination of Static Contact Angle*; UNE-EN 15802:2009; AENOR: Madrid, 2009.

(63) Rodriguez-Navarro, C.; Elert, K.; Ševčík, R. Amorphous and Crystalline Calcium Carbonate Phases during Carbonation of Nanolimes: Implications in Heritage Conservation. *CrystEngComm* **2016**, *18* (35), 6594−6607.

(64) Rodriguez-Navarro, C.; Kudłacz, K.; Cizer, Ö.; Ruiz-Agudo, E. Formation of Amorphous Calcium Carbonate and Its Transformation into Mesostructured Calcite. *CrystEngComm* **2015**, *17* (1), 58−72.

(65) Millan, A. Crystal Growth Shape of Whewellite Polymorphs: Influence of Structure Distortions on Crystal Shape. *Cryst. Growth Des.* **2001**, *1* (3), 245−254.

(66) Valentini, E.; Benincasa, A.; Tiano, P.; Fratini, F.; Rescic, S. *On Site Drilling Resistance Profiles of Natural Stones*; ICVBC: Florence, Italy,2008.

(67) Luque, A.; Cultrone, G.; Mosch, S.; Siegesmund, S.; Sebastian, E.; Leiss, B. Anisotropic Behaviour of White Macael Marble Used in the Alhambra of Granada (Spain). The Role of Thermohydric Expansion in Stone Durability. *Eng. Geol.* **2010**, *115* (3−4), 209−216.

(68) Benavente, D.; Martínez-Verdú, F.; Bernabeu, A.; Viqueira, V.; Fort, R.; García del Cura, M. A.; Illueca, C.; Ordóñez, S. Influence of Surface Roughness on Color Changes in Building Stones. *Color Res. Appl.* **2003**, *28* (5), 343−351.

(69) Urosevic, M.; Yebra-Rodríguez, A.; Sebastián-Pardo, E.; Cardell, C. Black Soiling of an Architectural Limestone during Two-Year Term Exposure to Urban Air in the City of Granada (S Spain). *Sci. Total Environ.* **2012**, *414*, 564−575.

(70) Wang, Z.; Volinsky, A. A.; Gallant, N. D. Crosslinking Effect on Polydimethylsiloxane Elastic Modulus Measured by Custom-Built Compression Instrument. *J. Appl. Polym. Sci.* **2014**, *131* (22), 1−4.

(71) Johnston, I. D.; McCluskey, D. K.; Tan, C. K. L.; Tracey, M. C. Mechanical Characterization of Bulk Sylgard 184 for Microfluidics and Microengineering. *J. Micromech. Microeng.* **2014**, *24* (3), No. 035017.

(72) Wen, J. Y.; Mark, J. E. Sol-Gel Preparation of Composites of Poly(Dimethylsiloxane) With Sio2 and Sio2/Tio2 and Their Mechanical-Properties. *Polym. J.* **1995**, *27*, 492−502.

(73) Tserepi, a D.; Vlachopoulou, M.-E.; Gogolides, E. Nanotexturing of Poly(Dimethylsiloxane) in Plasmas for Creating Robust Super-Hydrophobic Surfaces. *Nanotechnology* **2006**, *17* (15), 3977−3983.

(74) Xu, F.; Li, D.; Zhang, Q.; Zhang, H.; Xu, J. Effects of Addition of Colloidal Silica Particles on TEOS-Based Stone Protection Using n-Octylamine as a Catalyst. *Prog. Org. Coat.* **2012**, *75* (4), 429−434.

(75) Mosquera, M. J.; de los Santos, D. M.; Montes, A.; Valdez-Castro, L. New Nanomaterials for Consolidating Stone. *Langmuir* **2008**, *24* (6), 2772−2778.

(76) Matziaris, K.; Panayiotou, C. Tunable Wettability on Pendelic Marble: Could an Inorganic Marble Surface Behave as a "Self-Cleaning" Biological Surface? *J. Mater. Sci.* **2014**, *49* (5), 1931−1946.

(77) Sassoni, E.; Graziani, G.; Franzoni, E. Repair of Sugaring Marble by Ammonium Phosphate: Comparison with Ethyl Silicate and Ammonium Oxalate and Pilot Application to Historic Artifact. *Mater. Des.* **2015**, *88*, 1145−1157.

(78) Yang, F.; Liu, Y. Artificial Hydroxyapatite Film for the Conservation of Outdoor Marble Artworks. *Mater. Lett.* **2014**, *124*, 201−203.

(79) Ruiz-Agudo, E.; Álvarez-Lloret, P.; Ibañez-Velasco, A.; Ortega-Huertas, M. Crystallographic Control in the Replacement of Calcite by Calcium Sulfates. *Cryst. Growth Des.* **2016**, *16* (9), 4950−4959.